

HABITABLE ZONES AROUND MAIN-SEQUENCE STARS: DEPENDENCE ON PLANETARY MASS

Ravi kumar Kopparapu^{1,2,3,4,5}, Ramses M. Ramirez^{1,2,3,4}, James SchottelKotte⁶, James F. Kasting^{1,2,3,4}, Shawn Domagal-Goldman^{2,7}, Vincent Eymet⁸

ABSTRACT

The ongoing discoveries of extrasolar planets are unveiling a wide range of terrestrial mass (size) planets around their host stars. In this letter, we present estimates of habitable zones (HZs) around stars with stellar effective temperatures in the range 2600 K - 7200 K, for planetary masses between 0.1 M_{\oplus} and 5 M_{\oplus} . Assuming H₂O- (inner HZ) and CO₂- (outer HZ) dominated atmospheres, and scaling the background N₂ atmospheric pressure with the radius of the planet, our results indicate that larger planets have wider HZs than do smaller ones. Specifically, with the assumption that smaller planets will have less dense atmospheres, the inner edge of the HZ (runaway greenhouse limit) moves outward ($\sim 10\%$ lower than Earth flux) for low mass planets due to larger greenhouse effect arising from the increased H₂O column depth. For larger planets, the H₂O column depth is smaller, and higher temperatures are needed before water vapor completely dominates the outgoing longwave radiation. Hence the inner edge moves inward ($\sim 7\%$ higher than Earth's flux). The outer HZ changes little due to the competing effects of the greenhouse effect and an increase in albedo. New, 3-D climate model results from other groups are also summarized, and we

¹Department of Geosciences, Penn State University, 443 Deike Building, University Park, PA 16802, USA

²NASA Astrobiology Institute's Virtual Planetary Laboratory, P.O. Box 351580, Seattle, WA 98195, USA

³Penn State Astrobiology Research Center, 2217 Earth and Engineering Sciences Building University Park, PA 16802

⁴Center for Exoplanets & Habitable Worlds, The Pennsylvania State University, University Park, PA 16802

⁵Blue Marble Space Institute of Science, PO Box 85561, Seattle, Washington 98145-1561, USA

⁶Department of Astronomy & Astrophysics, The Pennsylvania State University, 525 Davey Laboratory, University Park, 16802, USA

⁷Planetary Environments Laboratory, NASA Goddard Space Flight Center

⁸Laboratoire d'Astrophysique de Bordeaux, Universite de Bordeaux 1, UMR 5804

argue that further, independent studies are needed to verify their predictions. Combined with our previous work, the results presented here provide refined estimates of HZs around main-sequence stars and provide a step towards a more comprehensive analysis of HZs.

Subject headings: planets and satellites: atmospheres

1. Introduction

Recent observational surveys have discovered several potential habitable zone (HZ) planet candidates (Udry et al. 2007; Vogt et al. 2010; Pepe et al. 2011a; Borucki et al. 2011; Bonfils et al. 2011; Borucki et al. 2012; Vogt et al. 2012; ?; Anglada-Escude et al. 2013), and it is expected that this number will greatly increase as time passes (Dressing & Charbonneau 2013; Kopparapu 2013; Gaidos 2013). Accordingly, the circumstellar HZ is defined as the region around which a terrestrial mass planet, with favorable atmospheric conditions, can sustain liquid water on its surface (Huang 1959; Hart 1978; Kasting et al. 1993; Selsis et al. 2007b; Kopparapu et al. 2013). Currently, more than 1600 extra-solar planetary systems have been detected and > 2700 additional candidate systems from the *Kepler* mission are waiting to be confirmed (Batalha et al. 2013; Lissauer et al. 2014; Rowe et al. 2014).

Recently Kopparapu et al. (2013) obtained new, improved estimates of the boundaries of the HZ by updating Kasting et al. (1993) model with new H_2O and CO_2 absorption coefficients from updated line- by-line (LBL) databases such as HITRAN 2008 (Rothman et al. 2009) and HITEMP 2010 (Rothman et al. 2010).

Several other recent studies used 3D global circulation models (GCMs) to study the potential habitability of specific systems (Wordsworth et al. 2010; Forget et al. 2013). Specifically, a recent study by Yang et al. (2013) proposed that stabilizing cloud feedback can expand the inner HZ (IHZ) to roughly twice the stellar flux found from 1D climate calculations for tidally locked planets or planets that are in synchronous rotation around low mass stars. The stabilizing feedback arises from an increase in the planetary albedo due to the presence of thick water clouds at the sub-stellar point. In contrast, Leconte et al. (2013) found that for a rapidly rotating planet similar to Earth around a Sun-like star, clouds have a *destabilizing* feedback on the long-term warming. This is because of the displacement of the cloud formation layer to higher altitudes, increasing the greenhouse effect of the clouds compared to the cooling effect caused by their albedo. While clouds provide a positive feedback in their model, Leconte et al. (2013) show that Earth’s troposphere is not saturated everywhere, and that these unsaturated regions radiate efficiently to space, thereby cooling

the planet. Consequently, they find that the IHZ is closer to the Sun, at 0.95 AU, than predicted by the 1-D model of Kopparapu et al. (2013). A similar study by Wolf & Toon (2013), using the 3D Community Atmosphere Model 3 (CAM3), also found that the inner edge can be as close as 0.93 AU for our Sun. These results highlight the importance of 3D GCMs in understanding the varying climate feedbacks associated with both tidally locked and rapidly rotating planets. Further studies using 3D models will be necessary to obtain a consensus on the location of the inner edge of the HZ.

Here, we consider planetary masses M_p between $0.1 M_\oplus \leq M_p \leq 5 M_\oplus$. The lower limit includes Mars-mass planets. The upper limit is based on the observation that the theoretical and observed mass-radius relationships have different slopes beyond $5M_\oplus$ (see §2), suggesting the accumulation of an increasingly significant gas envelope for planets with sizes larger than $5M_\oplus$.

The outline of the paper is as follows: In §2 we briefly describe our 1-D cloud-free climate model. In §3 we present results from our climate model and illustrate various HZ limits as a function of planetary mass. In §3.1, we provide an analytical equation to calculate HZs incorporating various 3D GCM results. We conclude in §4.

2. Model Description

We used a 1D, radiative-convective, cloud-free climate model from Kopparapu et al. (2013). We considered planets of masses $0.1 M_\oplus$ and $5 M_\oplus$, which were assumed to have H_2O - (IHZ) or CO_2 - (OHZ) dominated atmospheres with N_2 as a background gas. We explored the following cases: (1) N_2 partial pressure ($p\text{N}_2$) was varied for a fixed planet mass ($1 M_\oplus$) to study the effect of non-condensable background gas on the HZ limits, (2) N_2 background pressure was fixed at a low value of 0.01 bar for various planetary masses ($0.1, 1$ and $5 M_\oplus$) to study the effect of gravity alone and (3) N_2 pressure was scaled according to the planetary radius, accounting implicitly for the possible effect of planet size on volatile abundance.

For the last case, we assume that the amount of volatiles acquired by a planet during the late stages of its formation is proportional to the planet’s mass. We further assume that the fraction of these volatiles that are outgassed either during or after accretion is the same for all planets. We should caution that volatile delivery to a planet is stochastic in nature, and may be a weak function of planetary mass (Raymond et al. 2006, 2007). Still, this is the best assumption we can make in the absence of a rigorous theory of how planetary volatile content varies with planet mass.

The surface pressure, P_s , of a planet for this last case is then given by:

$$\frac{P_s}{P_s^o} = \frac{N_{col}}{N_{col}^o} \cdot \frac{g}{g_o} \quad (1)$$

where N_{col} is the N_2 atmospheric column mass density, which is atmospheric mass (scales with planetary mass, M_p) divided by the surface area of the planet¹, and g is the acceleration due to gravity. P_s^o , N_{col}^o and g_o are the corresponding values for Earth.

Both the terms on the right-hand side of Eq.(1) are proportional to M_p/R_p^2 , where R_p is the radius of the planet. Therefore, Eq.(1) can be written as:

$$\frac{P_s}{P_s^o} = \left(\frac{M_p}{M_o}\right)^2 \cdot \left(\frac{R_o}{R_p}\right)^4 \quad (2)$$

Recent studies on mass-radius relationship of exoplanets have shown that mass is not directly proportional to radius cubed; instead, it has a more complicated relationship (Fortney et al. 2007; Seager 2010). Therefore, for our study, we used the mass and radius values of known exoplanets from the exoplanets.org database (Wright et al. 2011) and obtained the following M-R relation:

$$\frac{M_p}{M_o} = 0.968 \left(\frac{R_p}{R_o}\right)^{3.2}, M_p < 5M_\oplus$$

Using this relation, the surface pressure in Eq.(2) can be written as:

$$\frac{P_s}{P_s^o} = 0.937 \left(\frac{R_p}{R_o}\right)^{2.40}, M_p < 5M_\oplus \quad (3)$$

The above equation suggests that larger planets should have thicker atmospheres. An upper limit of $5 M_\oplus$ is motivated by the observation that planets more massive than this limit seem to have a steeper slope in the M-R relation than the one predicted by Seager (2010) or Fortney et al. (2007) for Earth-like composition. For now we assume that planets with masses $> 5 M_\oplus$ are not rocky.

H₂O and CO₂ clouds were neglected in the model, but the effect of the former is accounted for by increasing the surface albedo, as done in previous climate simulations by the Kasting research group (Haqq-Misra et al. 2008; Ramirez et al. 2013).

¹In general, $N_{col} = \int_{z_1}^{z_2} \rho(z) \cdot dz$, where z is the atmospheric height, $\rho(z)$ is the mass density of the atmosphere. In essence, N_{col} is the mass per unit area of a column of atmosphere.

3. Results

In Fig. 1, we show the variation in the calculated outgoing longwave radiation (OLR), planetary albedo and the effective solar flux (S_{eff}) incident on the planet as a function of the surface temperature (top row), and CO₂ partial pressure (bottom row). Panels *a-b* and *c-d* correspond to the inner and outer edge of the HZ, respectively. All the calculations assume a Sun-like star. Fig. 1(a) shows the case where the background N₂ partial pressure (pN_2) is varied from 0.01 – 10 bar for a 1 M_⊕ planet. At lower surface temperatures (< 350 K), where the H₂O vapor is not a major constituent of the atmosphere, the net OLR is higher for lower pN_2 . The reason is that the pressure broadening by N₂ is not effective at lower pressures, and hence results in less IR absorption and an increase in OLR. Another way to look at it is that, to radiate the same amount of OLR, the surface temperature needs to be higher for larger pN_2 . At higher surface temperatures (> 350 K), water vapor dominates the atmosphere, the atmosphere becomes opaque IR radiation, and the OLR asymptotes to a limiting value of $\sim 280 \text{ Wm}^{-2}$. A similar calculation performed by Pierrehumbert (2010) shows a distinctive peak in the OLR for low pN_2 , whereas our model does not show this feature. A possible reason could be that we are using Ingersoll (1969) formulation to calculate the adiabat, and perform a finer sublevel integration to calculate the cold-trap accurately. Although, this feature does not affect our conclusions, a more thorough investigation is needed to resolve these discrepancies.

The planetary albedo (second panel) is higher for larger N₂ pressures due to the Rayleigh scattering arising from the higher amount of non-condensable gas. The net effect of both the OLR (F_{IR}) and planetary albedo (or the net absorbed solar flux, F_{SOL}) can be combined to obtain $S_{eff} = F_{IR}/F_{SOL}$, shown in the bottom panel. The inner edge of the HZ in our model is determined by the “runaway greenhouse limit”, where the limiting OLR (or S_{eff}) is reached and the ocean vaporizes completely. This replaces the “moist-greenhouse limit” where the stratosphere becomes wet, which defined the HZ inner edge in Kasting et al. (1993) and Kopparapu et al. (2013). The reason is two fold: (1) Both these limits occur in our model at S_{eff} values within 2% of each other, so the difference is minimal. And (2) Leconte et al. (2013) predict a much lower tropopause temperatures than that predicted by our 1D model, due to non-grey radiative effects and unsaturated regions that flatten the thermal profile in the troposphere. Consequently, their tropopause temperature can be as low as 115 K, as compared to the 200 K assumed in our inverse 1D calculations. Further independent analysis is needed to test the robustness of this result, as non-LTE (Local Thermodynamic Equilibrium) effects might also be important.

Since the asymptotic OLR is similar for different amounts of pN_2 , we conclude that the inner edge of the HZ is depends weakly on the background N₂ present in the atmosphere for

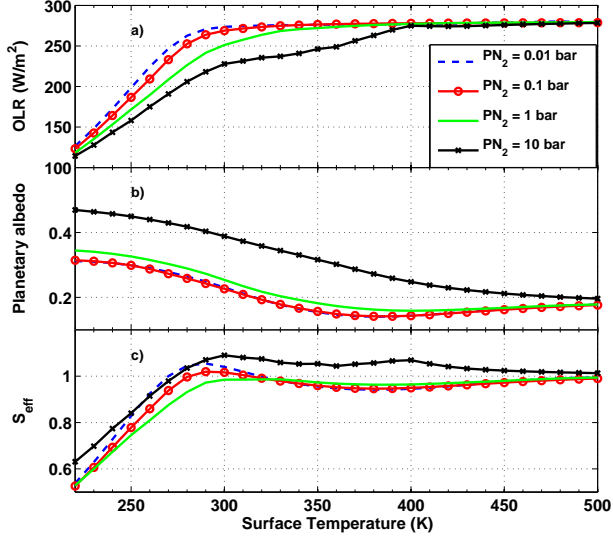
a given planet mass.

Fig. 1(b) illustrates the effect of planet mass (or gravity) on OLR, albedo and S_{eff} . Planetary masses of 0.1, 1 and 5 M_{\oplus} are chosen to encompass the terrestrial planet range. The background N_2 pressure is fixed at a low value of 0.01 bar to study the effect of gravity alone with minimal contribution from the non-condensable gas. Fig. 1(b) shows that the limiting OLR is higher for massive planets. This is because the H_2O column depth is larger for the 0.1 M_{\oplus} planet owing to its low gravity, which increases the greenhouse effect and reduces the OLR. The planetary albedo does not vary significantly, as the amount of N_2 present in the atmosphere is low². The net effect is that, for massive planets, S_{eff} is larger compared to low mass planets. Therefore, the inner edge of the HZ moves closer to the star for more massive planets.

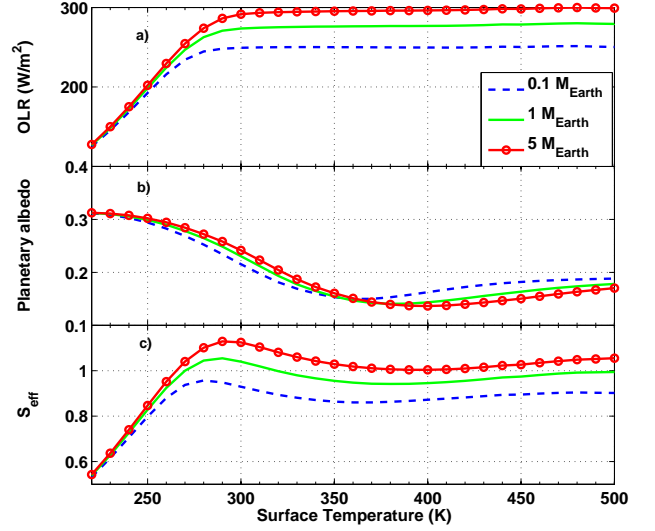
Figs. 1(c) and 1(d) show the results for the outer edge of the HZ, with the same variation in N_2 pressures (for 1 M_{\oplus}) and planetary mass (with $pN_2 = 0.01$ bar) as in Figs. 1(a) and 1(b). Fixing the surface temperature at 273 K, we varied the CO_2 partial pressure from 1 to 35 bars and calculated the corresponding radiative fluxes and planetary albedos. As with the inner edge case, less absorption occurs at low N_2 pressures because of ineffective pressure broadening, and this results in an increase in the OLR. This effect is augmented by an increase in planetary albedo at high pN_2 , resulting in decreased absorption of solar radiation. Thus, towards the left-hand side of Fig. 1(c), where pCO_2 is low, S_{eff} is considerably higher at low pN_2 . The HZ outer edge (the 'maximum greenhouse' limit) is determined by the minimum in S_{eff} . This boundary occurs at lower S_{eff} (i.e, further from the star) for large pN_2 (10 bar). For low enough pN_2 values, that minimum is governed by CO_2 , not N_2 (von Paris et al. 2013). Hence, the outer edge of the HZ does not change significantly for these low N_2 pressures.

As mentioned in section 2, we considered a third case where the background N_2 pressure is scaled according to the planetary mass. We consider this case to be a more realistic estimate for the non-condensable background gas concentration in a planetary atmosphere for the reasons outlined in section 2. Fig. 2 shows the inner (left panel) and outer (right panel) edge calculations for this case 3. These results can be understood by recognizing that they represent a combination of various cases shown in Fig. 1. For example, Fig. 1(a) shows that increasing pN_2 for a given planet mass shifts the peak OLR to higher temperatures due to pressure broadening (compare the 2 bar case with 0.01 bar). Also, Fig. 1(b) illustrates

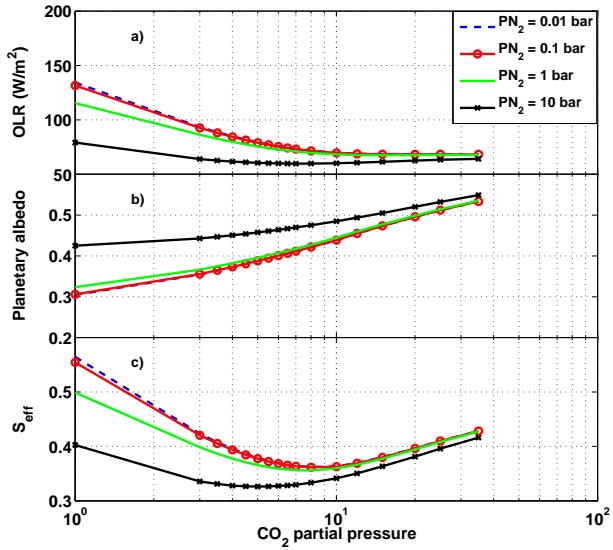
²For larger N_2 pressures, the albedo is higher for low mass planets because proportionately more nitrogen is put on the smaller planet which increases the Rayleigh scattering. But as the temperature increases, the albedo for all the planets asymptote to nearly the same value.



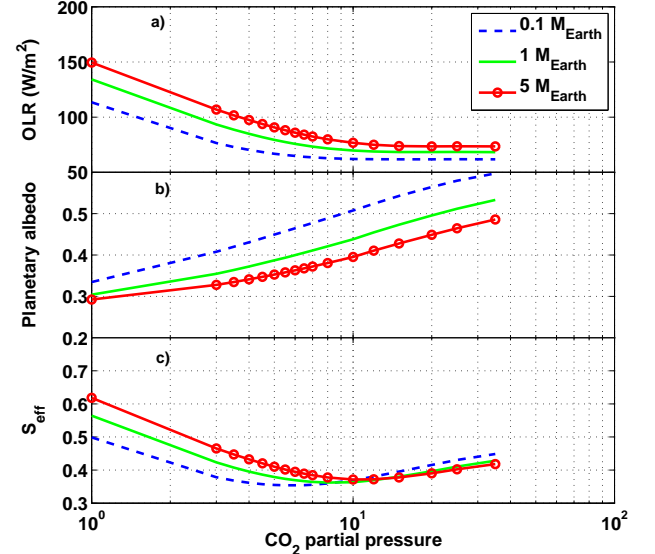
(a)



(b)



(c)



(d)

Fig. 1.— Variation in radiative fluxes and planetary albedo as a function of background N_2 partial pressure (panels (a) and (c)) and planetary mass (panels (b) & (d)). The top row is for the inner edge and the bottom row is for the outer edge of the HZ.

that the OLR is larger for a more massive planet due to smaller atmospheric column depth (for a given pN_2), and hence results in less IR absorption. Both these effects can be seen in Fig. 2(a), where both the planet mass and pN_2 are varied: The peak OLR shifts to higher temperatures because pN_2 is scaled, and the $5 M_{\oplus}$ planet has a higher OLR than a $0.1 M_{\oplus}$ planet which is a direct consequence of the results shown in Fig. 1(b).

Similar reasoning can be applied to the outer edge of the HZ (Fig. 2(b)). We showed in Figs. 1(c) and 1(d) that, there is not a significant change in S_{eff} for different planetary masses due to the competing effects of the greenhouse effect of CO_2 and the planetary albedo. This is reflected in the bottom panel of Fig. 2(b). Since the inner edge moves closer to the star for the super-Earth planet, while the outer edge changed little, we can conclude that larger (more massive) planets have wider habitable zones than do small ones.

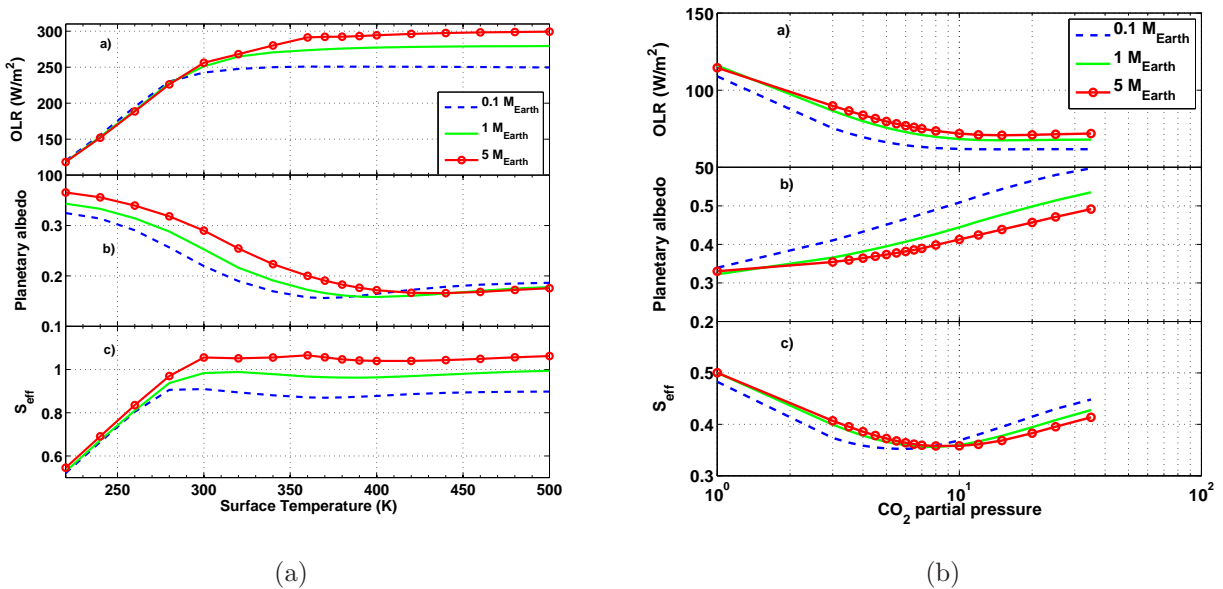


Fig. 2.— Similar to Fig. 1, but here pN_2 is scaled according to the planet mass as described by Eq.(3). The net effect is that the inner edge of the HZ (left-bottom panel) moves closer to the star for a massive planet and the outer edge of the HZ (right-bottom panel) changes little.

We should note that we found an error in our previously derived H_2O IR coefficients, which caused us to underestimate ($\sim 4\%$) the strength of the absorption by these gases at the inner edge. We have now corrected this error. As a result, the runaway greenhouse limit moves to lower stellar fluxes, and Earth now falls right on this limit suggesting that Earth should be in the runaway greenhouse state. This reflects our 1D model’s inability to realistically account for variations in relative humidity and clouds, which move IHZ to higher

stellar fluxes, as discussed earlier.

3.1. Variation of HZs With Planetary Mass

The results from the previous section can be extended to stars with different T_{eff} . Specifically, we use the results from pN_2 scaling with planetary mass to derive various HZ limits for stars with $2600 \text{ K} \leq T_{eff} \leq 7200 \text{ K}$.

By integrating the 1D and 3D model results, we have constructed the various HZ limits in Fig. 3. For rapidly rotating planets like the Earth, we scale the Leconte et al. (2013) inner edge limit with our value of the runaway greenhouse limit for different stars, and obtain a “conservative” estimate of the inner edge of the HZ (green curve). Note that Earth is well inside the HZ in this figure, as it should be, because the Leconte et al. (2013) runaway greenhouse limit occurs at a higher stellar flux.

For cool stars ($T_{eff} \leq 4500 \text{ K}$), the inner HZ is a function of tidal locking radius (Edson et al. (2011), dashed and solid black line in Fig. 3 assuming 4.5 Gyr tidal lock timescale). The Yang et al. (2013) GCM models considered an M-star with $T_{eff} = 3400\text{K}$ and a K-star with $T_{eff} = 4500\text{K}$. We show their model results in Fig.3 for both synchronously rotating and a 6:1 spin-orbit resonance case. This result needs to be verified with further studies.

A conservative estimate of the outer edge of the HZ is defined by the maximum greenhouse limit (blue solid curve). The actual outer edge could be further out if additional greenhouse gases (e.g., H_2) are present (Pierrehumbert & Gaidos 2011). The outer edge does not vary significantly for different planetary masses. The change in the stellar flux at the inner edge of the HZ, compared to Earth, is $\sim 10\%$ for $0.1 M_\oplus$ and $\sim 7\%$ for $5 M_\oplus$ in our model.

We provide parametric equations to calculate HZs:

$$S_{eff} = S_{eff\odot} + aT_\star + bT_\star^2 + cT_\star^3 + dT_\star^4 \quad (4)$$

where $T_\star = T_{eff} - 5780 \text{ K}$ and the coefficients are listed in Table 1. The corresponding habitable zone distances can be calculated using the relation:

$$d = \left(\frac{L/L_\odot}{S_{eff}} \right)^{0.5} \text{ AU} \quad (5)$$

where L/L_\odot is the luminosity of the star compared to the Sun.

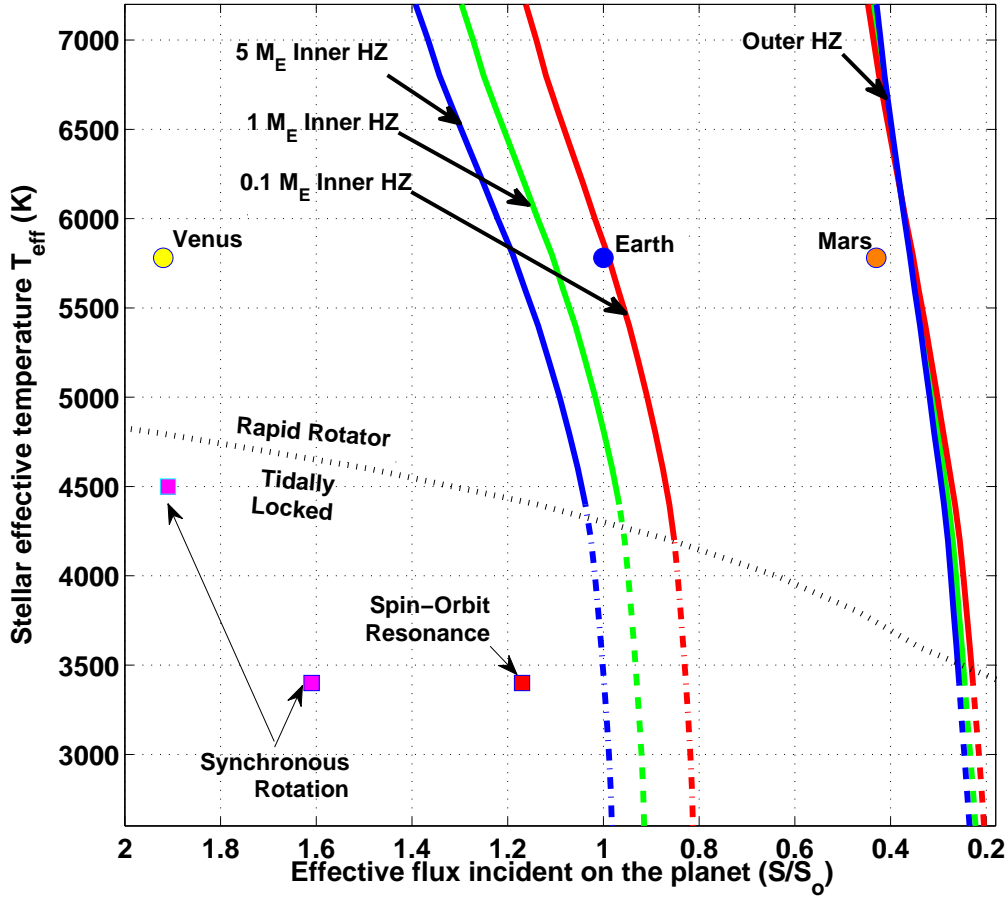


Fig. 3.— HZ limits for different planetary masses. The inner HZ for Earth (green curve) is scaled with the Leconte et al.(2013) inner HZ for the Sun, using our runaway greenhouse limit. The outer HZ is the maximum greenhouse limit. The tidal locking radius (black dot), assuming a 4.5 Gyr tidal locking timescale, separates rapidly rotating planets with tidally locked ones. The inner-edge limits for tidally locked planets around cool stars from Yang et al. (2013) are also shown (colored squares).

4. Conclusions

The HZ boundaries change as a function of planetary mass and the amount of background N_2 gas. The conservative HZ limits for more massive planets should be wider than those for low mass planets if the atmospheric column depth scales with planet radius, as assumed here. The results summarized here are only a step towards a more comprehensive analysis of HZ boundaries. Further work with 3D climate models will be needed to accurately calculate the habitable zones around different types of stars.

A FORTRAN code is available with the online version of the paper. An interactive webpage to obtain HZs is available at: <http://www3.geosc.psu.edu/~ruk15/planets/> or at <http://depts.washington.edu/naivpl/content/hz-calculator>.

The authors thank an anonymous reviewer whose comments greatly improved the manuscript. R. K, R. R, J.F.K and S.D.G gratefully acknowledge funding from NASA Astrobiology Institute's Virtual Planetary Laboratory lead team, supported by NASA under cooperative agreement NNH05ZDA001C, and the Penn State Astrobiology Research Center. V.E. acknowledges the support of the European Research Council (Starting Grant 209622: E3ARTHS). The Center for Exoplanets and Habitable Worlds is supported by the Pennsylvania State University, the Eberly College of Science, and the Pennsylvania Space Grant Consortium. R.K and R.R contributed equally to this work.

Table 1: Coefficients to be used in Eq.(4). The coefficients for recent Venus, Maximum Greenhouse and early Mars are same for all the planetary masses. For $5 M_{\oplus}$ and $0.1 M_{\oplus}$, the background N_2 pressure is scaled according to the planetary mass. An ASCII file containing these coefficients can be downloaded in the electronic version of the paper.

Constant	Recent Venus	Runaway Greenhouse	Maximum Greenhouse	Early Mars
$S_{eff\odot}$ ($1 M_{\oplus}$)	1.776	1.107	0.356	0.32
$S_{eff\odot}$ ($5 M_{\oplus}$)	–	1.188	–	–
$S_{eff\odot}$ ($0.1 M_{\oplus}$)	–	0.99	–	–
a ($1 M_{\oplus}$)	2.136×10^{-4}	1.332×10^{-4}	6.171×10^{-5}	5.547×10^{-5}
a ($5 M_{\oplus}$)	–	1.433×10^{-4}	–	–
a ($0.1 M_{\oplus}$)	–	1.209×10^{-4}	–	–
b ($1 M_{\oplus}$)	2.533×10^{-8}	1.58×10^{-8}	1.698×10^{-9}	1.526×10^{-9}
b ($5 M_{\oplus}$)	–	1.707×10^{-8}	–	–
b ($0.1 M_{\oplus}$)	–	1.404×10^{-8}	–	–
c ($1 M_{\oplus}$)	-1.332×10^{-11}	-8.308×10^{-12}	-3.198×10^{-12}	-2.874×10^{-12}
c ($5 M_{\oplus}$)	–	-8.968×10^{-12}	–	–
c ($0.1 M_{\oplus}$)	–	-7.418×10^{-12}	–	–
d ($1 M_{\oplus}$)	-3.097×10^{-15}	-1.931×10^{-15}	-5.575×10^{-16}	-5.011×10^{-16}
d ($5 M_{\oplus}$)	–	-2.084×10^{-15}	–	–
d ($0.1 M_{\oplus}$)	–	-1.713×10^{-15}	–	–

REFERENCES

- Anglada-Escude, G., Tuomi, M., Gerlach, E. et al. 2013. accepted to A&A, arXiv:1306.6074
- Batalha, N. M., Rowe, J. F., Bryson, S. T. et al. 2012. *ApJS*, 204, 24
- Bonfils, X., Delfosse, X., Udry, S. et al. 2011. submitted A&A, arXiv:1111.5019
- Borucki, W. J., Koch, D. G., Basri, G. et al. 2011. *ApJ*, 736, article id. 19
- Borucki, W. J., Koch, D. G., Batalha, N. et al. 2012. *ApJ*, 745, article id. 120
- Dressing, C., & Charbonneau, D. 2013. *ApJ*, 767, 1
- Edson, A., Lee, S., Bannon, P. et al. 2011. *Icarus*, 212, 1
- Forget, F., Wordsworth, R. W., Millour, E. et al. 2013 *Icarus*, 222, 1
- Fortney, J. J., Marley, M. S., Barnes, J. W. 2007. *ApJ*, 659, 1661
- Gaidos, E. 2013, *ApJ*, 770, 90
- Haqq-Misra, J. D., Domagal-Goldman, S. D., Kasting, P. J. & Kasting, J. F. 2008. *Astrobiology*, 8, 1127
- Hart, M. H. 1978, *Icarus*, 33, 23
- Huang, S. S. 1959, *American Scientist*, 47, 397
- Ingersoll, A. P. 1969, *JAtS*, 26, 1191
- Kasting, J., F., Whitmire, D., P., & Reynolds. R. T. 1993, *Icarus*, 101, 108
- Kopparapu, R. K., Ramirez, R., Kasting, J. F., Eymet, V., Robinson, T. D., Mahadevan, S., Terrien, R. C., Domagal-Goldman, S. D., Meadows, V., & Deshpande, R. 2013, *ApJ*, 765, 131
- Kopparapu, R. K. 2013. *ApJ*, 767, 1
- Leconte, J., Forget, F., Charnay, B., Wordsworth, R., & Pottier, A. 2013. *Nature*, 504, 268
- Lissauer, J. J., Marcy, G. W., Bryson, S. T., et al., 2014. *ApJ*, 784, 44
- Pierrehumbert, R. T., & Gaidos, E. 2011. *ApJ*, 734, L13
- Pepe, F., Lovis, C., Segransan, D. et al. 2011a. *A&A*, 534, A58

- Ramirez, R. M., Kopparapu, R., Kasting, J. F. et al. 2013, *Nature Geoscience*, 7, 59
- Raymond, S. N., Mandell, A. M., Sigurdsson, S. 2006. *Science*. 313, 5792
- Raymond, S. N., Quinn, T., Lunine, J. I. 2007. *Astrobiology*. 7, 1
- Rothman, L. S., Gordon, I. E., Barber, A., et al. 2008. *JQSRT*, 110, 533
- Rothman, L. S., Gordon, I. E., Barber, A., et al. 2010. *JQSRT*, 111, 2139
- Rowe, J. F., Bryson, S. T., Marcy, G. W., et al. 2014. *ApJ*, 784, 45
- Selsis, F. et al. 2007b. *A&A*, 476, 137
- Pierrehumbert, R. T. 2010. *Principles of Planetary Climate*, Cambridge University Press
- Seager, S. 2010. *Exoplanets*, The University of Arizona Press
- Udry, S., Bonfils, X., Delfosse, X. et al. 2007. *A&A*. 469, L43
- Vogt, S. S., Butler, R. P., & Rivera, E. J. et al. 2010. *ApJ*, 723, 954
- Vogt, S. S., Butler, P., & Haghighipour, N. 2012. *Astronomische Nachrichten*, 333, 561
- Von Paris, P., Grenfell, J. L., Rauer, H., & Stock, J. W. 2013, *Planetary and Space Science*, 82, 149
- Wolf, E., & Toon, E. 2013. *Geophysical Research Letters*. 41, doi:10.1002/2013GL058376
- Wordsworth, R., & Pierrehumbert, R. 2013. *Science*, 339, 64
- Wordsworth, R., Forget, F., & Eymont, V. 2010, *Icarus*, 210, 2, 992
- Wright, J. T., Fakhouri, O., Marcy, G. W. et al. 2011. *PASP*, 123, 412
- Yang, J., Cowan, N. B., & Abbot, D. S. 2013. *ApJ*, 771, L45